In vivo multi-modality photoacoustic and pulse echo tracking of prostate tumor growth using a window chamber

Daniel R. Bauer*, Ragnar Olafsson, Leonardo G. Montilla, Russell S. Witte
Dept. of Radiology, University of Arizona, Tucson, AZ 85724
*dan.bauer5@gmail.com

ABSTRACT

Understanding the tumor microenvironment is critical to characterizing how cancers operate and predicting how they will eventually respond to treatment. The mouse window chamber model is an excellent tool for cancer research, because it enables high resolution tumor imaging and cross-validation using multiple modalities. We describe a novel multimodality imaging system that incorporates three dimensional (3D) photoacoustics with pulse echo ultrasound for imaging the tumor microenvironment and tracking tissue growth in mice. Three mice were implanted with a dorsal skin flap window chamber. PC-3 prostate tumor cells, expressing green fluorescent protein (GFP), were injected into the skin. The ensuing tumor invasion was mapped using photoacoustic and pulse echo imaging, as well as optical and fluorescent imaging for comparison and cross validation. The photoacoustic imaging and spectroscopy system, consisting of a tunable (680-1000nm) pulsed laser and 25 MHz ultrasound transducer, revealed near infrared absorbing regions, primarily blood vessels. Pulse echo images, obtained simultaneously, provided details of the tumor microstructure and growth with 100-μm^3 resolution. The tumor size in all three mice increased between three and five fold during 3+ weeks of imaging. Results were consistent with the optical and fluorescent images. Photoacoustic imaging revealed detailed maps of the tumor vasculature, whereas photoacoustic spectroscopy identified regions of oxygenated and deoxygenated blood vessels. The 3D photoacoustic and pulse echo imaging system provided complementary information to track the tumor microenvironment, evaluate new cancer therapies, and develop molecular imaging agents *in vivo*. Finally, these safe and noninvasive techniques are potentially applicable for human cancer imaging.

Keywords: optoacoustic, ultrasound, window chamber, prostate cancer, green fluorescent protein, GFP, cancer biology, angiogenesis

1. INTRODUCTION

Prostate cancer is an aggressive disease that has high morbidity and mortality rates. It is the most commonly diagnosed invasive cancer and a leading cause of death in men with cancer[1-4]. The American Cancer Society estimates that in the United States in 2009 over 190,000 cases will be diagnosed and that over 27,000 men will die of prostate cancer[5]. An estimated 1 in 6 men will develop the disease, making it the second leading cause of death among men in the U.S. Improved detection and early diagnosis of prostate cancer would aid in intervention and treatment of the disease.

Photoacoustics (PA) is an emerging modality in biomedical research that exhibits great potential for cancer detection and characterization. In PA imaging, the biological sample is illuminated with light, typically in the form of a high energy pulsed laser. As light penetrates the skin, its energy is partially absorbed and converted to heat causing thermoelastic expansion and the generation of acoustic waves. These ultrasound waves are proportional to the spatially varying optical absorption coefficient of the material, resulting in a 3D image of the relative optical absorption of the sample. Because this modality detects ultrasound waves, depth information of the sample is obtained from the speed of sound in the sample, an added benefit not usually seen with optical techniques. Photoacoustic imaging can offer penetration depths of several millimeters with visible radiation and several centimeters with NIR light. Also, high resolution pulse echo ultrasound (PE) can be captured simultaneously using the same transducer. Collecting PE and PA data concurrently is useful because they provide very different information about the tumor microenvironment. The PE signal is generated from acoustic reflections, such as those from tissue interfaces or small biological structures. Conversely, PA contrast is generated from areas of spatially varying optical absorption, such as tumor vasculature and hemoglobin content in the blood. These modalities, therefore, offer complementary contrast.

Photons Plus Ultrasound: Imaging and Sensing 2010, edited by Alexander A. Oraevsky, Lihong V. Wang,
Proc. of SPIE Vol. 7564, 75643B · © 2010 SPIE · CCC code: 1605-7422/10/$18 · doi: 10.1117/12.843875

Downloaded from SPIE Digital Library on 04 Apr 2010 to 150.135.114.25. Terms of Use: http://spiedl.org/terms

This study involved a window chamber that was clamped to the skin of mice using a custom holder and transparent glass coverslip. The tissue was sandwiched between the mouse's skin on one side and the coverslip on the other. This standard window chamber model offers several key benefits to study cancer and has been previously used with several imaging modalities, including fluorescent microscopy[6-8], magnetic resonance[9-12], electrode imaging[13], biological polarimetry[14] and computed tomography[15]. The window chamber model is advantageous, because it allows for long-term studies (several weeks) to analyze the tumor microenvironment and track tumor growth. The thin layer of the skin flap (<1 cm) enables transmission mode photoacoustic imaging. Overall, the technique is an excellent model for imaging tumor growth, exploring models of the tumor microenvironment, testing novel cancer therapies and developing imaging technologies and complementary contrast agents. Although there have been other studies conducted using the window chamber to study prostate cancer, this is the first study to implement the window chamber model with simultaneous high resolution PE and PA to monitor prostate tumor growth for several weeks, providing maps of the tumor microstructure and vasculature system. For comparison and cross-validation, the tumor was also imaged with fluorescent and optical modalities.

2. METHODS AND MATERIALS

2.1 SCID Mice Protocol

Three severe combined immunodeficiency (SCID) mice were used in this study. All three had a window chamber fitted onto the loose skin on their back, as seen in Figure 1 (right). One side of the skin flap had exposed skin (skin side) while the other side had a glass coverslip placed on it (coverslip side). PC-3 prostate tumor cells expressing green fluorescent protein (GFP) were implanted into the dorsal skin flap and monitored over the course of the subsequent 4 weeks (starting one week after the injection of tumor cells). Mice were cared for in accordance with protocols approved by the Institutional Animal Care and Use Committee (IACUC) at the University of Arizona and maintained in a sterile clean room facility in individual cages with controlled temperature and humidity.

On imaging days the mice were transported to the laboratory and anesthetized with an isoflurane flow system. The mouse was placed in a gas chamber and 2% isoflurane was administered using O_2 with a flow rate of approximately 1 liter / min until the mouse was fully anesthetized. The mouse was then moved to the imaging setup, where the ultrasound transducer was placed in a water tank facing the skin side of the mouse (separated by an acoustic membrane). Hypoallergenic index matching gel (Parker Aquasonic 100) was placed on the skin side of the window chamber to provide acoustic coupling. The mouse was placed on a custom built pad so that the window chamber would fit into the appropriate position with respect to the water bath and incident laser light. Once the mouse was in position, isoflurane was delivered to the animal using a cone shaped end piece to fit around the head of the mouse. The percent isoflurane was then reduced to ~1% and Puralube® gel was placed over the eyes to prevent damage. Furthermore, the mouse was kept warm with a custom built pad, fitted with a heating element, and an overhead heating lamp.

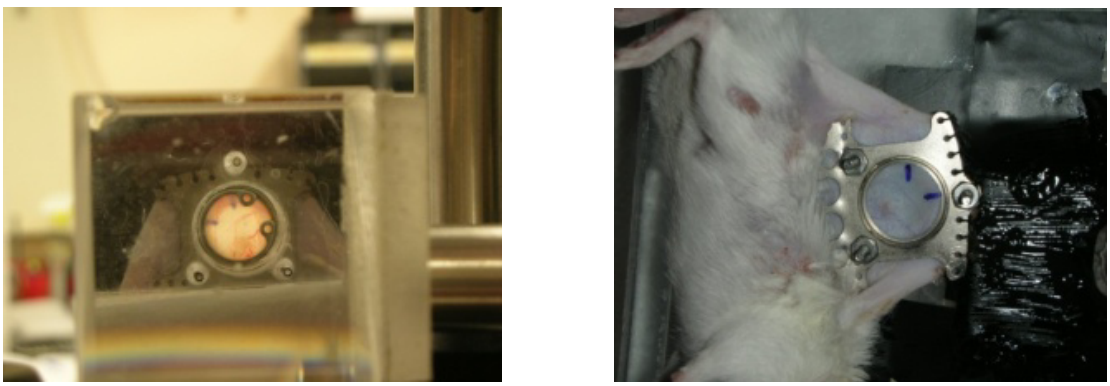

Figure 1. (left) Photograph from Day 9 (post implantation) of mouse R1's window chamber from the coverslip side as seen through right angle prism used in PAI setup. (right) Picture of mouse R1 on Day 9 with window chamber from the skin side. The side of the mouse displayed has exposed skin with two ink reference marks on skin surface. The three screws on the chamber were used to mount the chamber to the imaging apparatus.

Downloaded from SPIE Digital Library on 04 Apr 2010 to 150.135.114.25. Terms of Use: http://spiedl.org/terms

2.2 PE and PA Imaging Setup

The PA and PE imaging system is displayed in Figure 2. The setup involved a tunable pulsed laser source (Surelite I-20, Continuum, Inc, 5 nsec, ~20 mJ/pulse, tunable 680-1000 nm, 20 Hz) that was synchronized with the data acquisition system and motor stages (Velmex, Inc), such that the raw photoacoustic signal detection at each position could be synchronized with the firing of the laser. The laser light passed through a two-lens optical beam expander to increase the beam size to the diameter of the window chamber (~12 mm). Just prior to illuminating the water tank, the beam was passed through a diffuser, as seen in Figure 2, in order to improve beam uniformity. A 25 MHz focused transducer (Olympus V324) with a focal length of 12.7 mm was connected to a pulser/receiver (Olympus Panametrics-NDT 5900PR). A single transmit pulse was synchronized with the laser firing in order to simultaneously detect both the pulse echo and photoacoustic signals (separated by the one way vs. two way travel of the acoustic waves generated by each modality). The transducer was raster scanned across the tumor in both lateral dimensions to produce a 3D data set of the tumor microenvironment. In general, a rectangular region of interest ($x \approx 6$ mm, $y \approx 14$ mm) was scanned with spacing of $\Delta x = 100\mu m$ and $\Delta y = 47.6\mu m$.

The window chamber of the mouse was placed in the path of the laser and just below the water tank. An index matching gel was coupled between the window chamber and the water tank in order to prevent acoustic reflections off an air-water interface. The transducer was placed in the water bath and connected to the pulser/receiver. The height of the transducer relative to the window chamber was adjusted to focus the transducer between the skin and coverslip. This was accomplished by placing the transducer's focus between the large PE signals generated by the coverslip and upper tissue interface. The transducer was then connected to a fast data acquisition board (PDA12, Signatec Inc) on the computer via the pulser/receiver so that the signal could be digitized at 62.5 MHz and at 12 bits and stored on a PC. The data was then filtered, averaged and analyzed in MATLAB® (Mathworks, Inc).

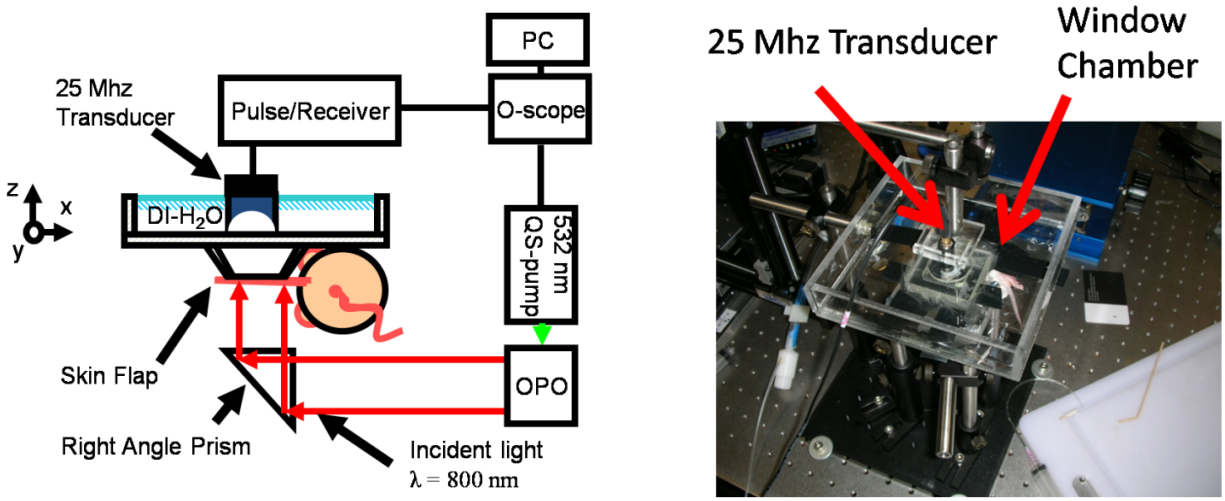

Figure 2. (left) Schematic diagram of the imaging setup. (right) Photograph of setup showing 25 MHz transducer, water bath, and tail of the mouse.

2.3 Optical and Fluorescent Imaging Setup

Optical and fluorescent images were taken using high resolution confocal microscopy. A custom built plastic holder was made with appropriate holes for the screws on the skin side of the window chamber as seen in Figure 1 (right). In the same manner as mentioned earlier, the mice were fully anesthetized before and during imaging. The mouse, with the window chamber placed in the holder, was then placed on the microscope stage. Stage clips were used to fasten the holder to the stage such that the window chamber was centered on the microscopes field of view. Trans-illumination images were taken by illuminating the bottom of the skin flap with white light. Additionally, illuminating the skin with ~400 nm light, fluorescent images were captured of the tumor which was composed of GFP cells. In both cases, the window chamber was imaged at 1x magnification to see the whole window chamber and 2x magnification to exemplify detail.

Downloaded from SPIE Digital Library on 04 Apr 2010 to 150.135.114.25. Terms of Use: http://spiedl.org/terms

2.4 Data Processing

The stored radiofrequency data was demodulated to form a 2D image by using a modified Fourier transform in conjunction with a Hanning filter centered at 25 MHz. The XY planes were then filtered with a low order median filter followed by a smoothing filter to reduce noise. The individual 2D slices were then combined into a 3D data set for further analysis.

As a means to track tumor growth over time using the PE data, an automated volume tracking algorithm was developed, as can be seen in Figure 3. The program was based on image segmentation techniques to enhance borders, so that clear tissue boundaries could be determined. The data was thresholded to help reduce noise, and boundaries of each the acoustic membrane and coverslip were determined using the segmentation algorithm. A continuous boundary was formed by enhancing weak boundaries using a series of dilated masks intended to connect areas of weak PE signal. After a boundary was determined, a contour following algorithm was used to calculate the pixels of the tissue-gel interface and coverslip, which was assumed to be the lower boundary of the skin. The region between the coverslip and skin-gel interface was then calculated. The effective area of tissue in a given plane was determined by iteratively applying the algorithm. The tissue volume was determined by taking into account the appropriate inter-plane scanning distance.

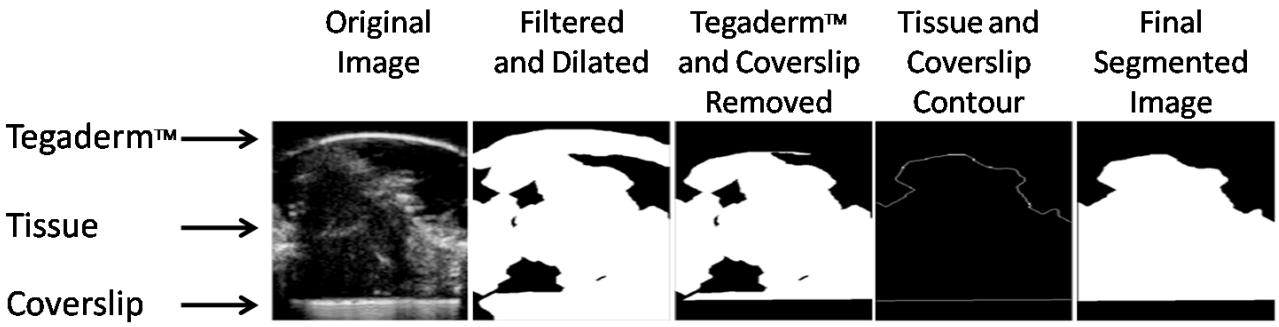

Figure 3. Graphical representation of pulse echo image segmentation. Displays depth slice of mouse R0 on Day 23.

Additionally, an image segmentation algorithm was developed to determine the size of the fluorescing tumor. Because the GFP signal was seen to be significantly stronger than background, the algorithm utilizes a user input threshold value which converts an intensity image into a binary image. In this manner only GFP pixels will be thresholded high and the total number of high pixels is calculated. The total area of the window chamber is known so that the area per pixel can be calculated and multiplied by the total number of thresholded pixels to yield an approximate fluorescing tumor area.

3. RESULTS AND DISCUSSION

3.1 Optical and Fluorescent Imaging

Optical and fluorescent images of the GFP transfected tumors were used as a standard to characterize the tumor's physical development. The fluorescence data is useful because the tumor cells contain GFP, so that a fluorescent signal can be directly correlated to the presence of tumor cells. Fluorescence, however, does have limitations, such as limited depth information can be obtained because the fluorescence is generally integrated along the depth direction by the detection camera.

Figure 4 depicts a series of images near the tumor of mouse R2. The optical image of the window chamber (coverslip side) has been magnified in the trans-illumination and fluorescent images to display more detail. In the trans-illumination image, a large blood vessel can be seen passing through the middle of the tumor, which appears dark compared to the surrounding tissue. The fluorescent image clearly identifies the location of the tumor cells expressing GFP. In each image the tumor vasculature, as well as the size and location of the tumor, can be readily determined. The fluorescent thresholding algorithm was used to calculate the size of the fluorescing tumor. The GFP thresholded result for mouse R2 on Day 12 is displayed in Figure 4 (right) and was analyzed to compute the tumor size.

Downloaded from SPIE Digital Library on 04 Apr 2010 to 150.135.114.25. Terms of Use: http://spiedl.org/terms

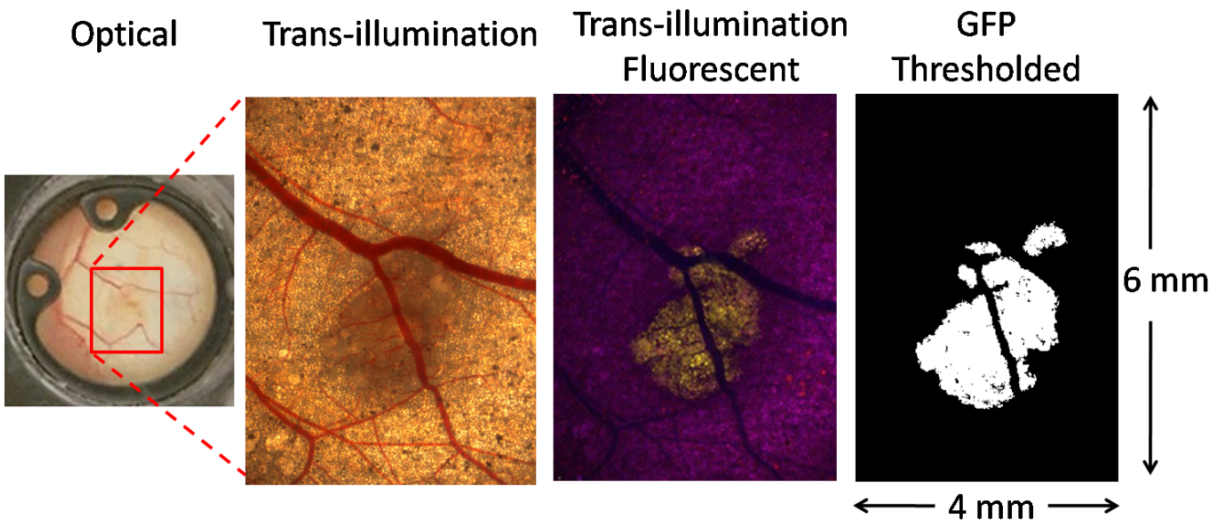

Figure 4. (Left to Right), displays the optical (Day 9), trans-illumination (Day 12), fluorescent (Day 12), and thresholded fluorescent image (Day 12) of mouse R2. Red scale box has dimensions of approximately 4 mm x 6 mm.

The growth of each mouse's tumor, calculated using the GFP thresholding algorithm, can be seen below in Figure 5. Mouse R1 and R2 exhibit a roughly linear increase in overall GFP distribution. Mouse R0's tumor appears to decrease in size during the last week of the study. This could be the result of a necrotic core or the animal's own immune system fighting off the tumor which is not uncommon in cancer SCID mice window chamber models.

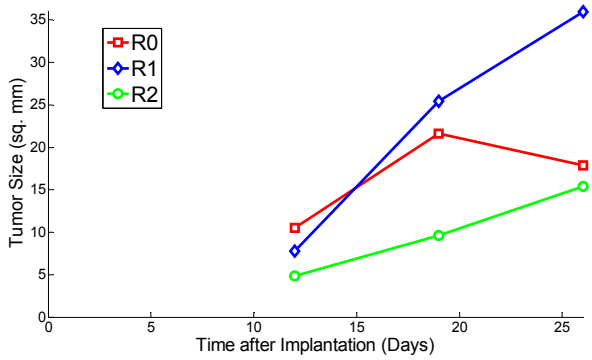

Figure 5. Tumor growth of three mice: R0 (red), R1 (blue), and R2 (green) in terms of fluorescent signal as determined from the fluorescent thresholding algorithm.

3.2 PE and PA Imaging

An example of PA and PE tracking of tumor growth is shown in Figure 6. A depth slice near the tumor center is displayed. The growth of the tumor reveals interesting growth characteristics of the tumor. The relatively small difference in physical tumor size between Days 9 and 16 should be noted as the tumor only grows approximately 1 mm in the depth direction. The latter two records (Day 23 and 29), indicate dramatic growth in tumor size, although in different directions. Day 23 shows a large growth spurt along the depth direction when compared to Day 16. The following data point at Day 29 shows almost no growth in the depth direction but a significant amount of lateral tumor development. These results indicate that the tumor does not grow in a uniform or well established manner, possible due to the tumor boundary constraints posed by the stiff coverslip on one side and the compressed skin on the other. Interestingly, as the tumor progresses it develops a hyperechoic outer tissue ring surrounding a hypoechoic inner core (Figure 6, right).

Downloaded from SPIE Digital Library on 04 Apr 2010 to 150.135.114.25. Terms of Use: http://spiedl.org/terms

The PA images provide insight into the tumor vasculature network and allow for comparisons between the PE and optical images. In the PA images the large signal to the right of the tumor protrusion can be attributed to a fiducial ink mark placed on the skin of the animal on Day 23.

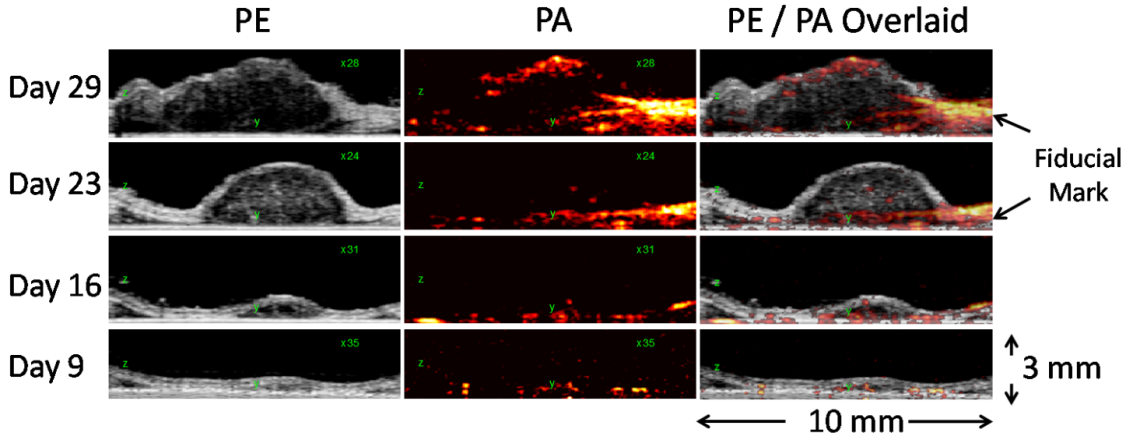

Figure 6. From left to right column: PE image, PA image, and both co-registered and superimposed on a common plot for mouse R2. The vertical axis represents depth and the horizontal axis lateral dimension. Each slice occurs at the approximate tumor center. The large PA signal on the right is a fiducial mark placed on the skin of the animal.

The results from the volumetric analysis of tissue growth are shown in Figure 7 (left). It was assumed that most of the overall increase in size or volume was attributed to tumor growth or a resulting byproduct of the tumor, such as edema or inflammation. As expected, all three mice demonstrated a general increase in tissue volume over the course of the experiment. It should also be noted that all three mice exhibit a faster rate of tumor increase after Day 16. No data point is available for mouse R1 at 29 days post implantation because the mouse died prematurely. Each mouse's tumor can be seen, as observed through the coverslip on Day 23, in Figure 7 (middle). A corresponding depth slice from the same day, and centered on the tumor, is shown in Figure 7 (right). The tumor size of mouse R0 and R1 appears significantly larger than that of R2, a result that is reiterated in the PE volumetric analysis.

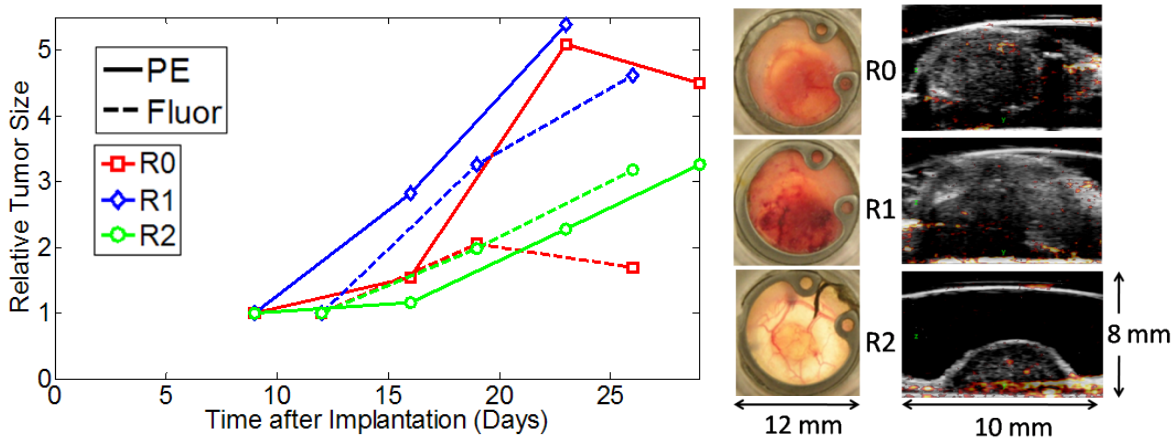

Figure 7. (left) Volumetric tissue growth over region of interest centered on each tumor, respectively. Tumor implantation corresponds to Day = 0. Both modalities have been normalized to their respective initial measurements. (middle) Photograph of the window chambers for each mouse (coverslip side) on Day 23. (right) Approximate center depth plane of tumor on Day 23 PE (gray) and PA (hot).

Tumor growth determined from fluorescent and PE imaging are displayed together in Figure 7 (left). Each respective signal has been normalized to their initial conditions. Placed on a relative scale, mouse R1 and R2 demonstrated a

Downloaded from SPIE Digital Library on 04 Apr 2010 to 150.135.114.25. Terms of Use: http://spiedl.org/terms

roughly linear increase in both overall tissue growth and GFP distribution as their plots scale together. Note that mouse R0 in Figure 7 demonstrates a reduction in tumor size over the last week of the study. This finding is supported by the fluorescent results from Figure 5. There are several plausible explanations for the decrease in tumor size. The optical and fluorescent images of the tumor show that it grows rapidly toward the edge of the window chamber such that by Day 29 it is near the border of the window chamber. It is possible that the tumor was able to spread outside of the window chamber so that tracking its growth would not yield an accurate result. Conversely, and potentially more likely, this outcome could be explained by the mouse's own immune system fighting off the tumor cells. Despite being a SCID mouse, it's possible that its immune system started to fight off the tumor. Although no absolute comparisons between GFP distribution and tissue volume can be deduced from Figure 7, it provides a useful tool to enable co-validation between fluorescent and ultrasound imaging regarding the growth of the tumor.

3.3 PA Imaging and Comparison with other Modalities

There are several significant advantages to multimodality imaging because each technique yields complementary information regarding the tumor microenvironment. When combined with ultrasound imaging, other modalities, such as photoacoustics, optical, and fluorescent imaging, can be used to further characterize the tumor environment, as well as providing cross modality comparison and corroboration of findings.

Figure 8 is an example of multimodality imaging, depicting optical, fluorescent, PA, and PE imaging techniques of the same mouse. The window chamber photograph is used as a reference when comparing the ultrasound and fluorescent images. In the window chamber photograph, the tumor can be seen in the center of the red scale box as slightly darker than the surrounding tissue. The fluorescent, PA and PE images are of particular interest in this example. In the trans-illumination fluorescent image, many blood vessels are visualized, with several of them branching in or around the tumor. The same blood vessels are resolved using PA imaging because blood has a larger optical absorption compared to nearby tissue. Whereas fluorescent images are a 2D projection of the fluorescent signal, PA imaging offers the added benefit of depth information so that the location of blood vessels can be imaged in three dimensions. To compare the 3D PA images with the 2D Fluorescent image, the data set was reduced to a 2D image through a maximum PA intensity projection along the depth direction to yield the PA image in Figure 8. This allows the user to visualize the strongest signals independent of depth position. A 3D rendering of the tumor's vascular network provides additional detail of the tumor vasculature (not displayed in this example). In the PA image, blood vessels are clearly detected, consistent with the images produced by the optical modalities. Additionally, the PA signal has the added benefit of mapping deep vessels that cannot be clearly resolved from the skin surface.

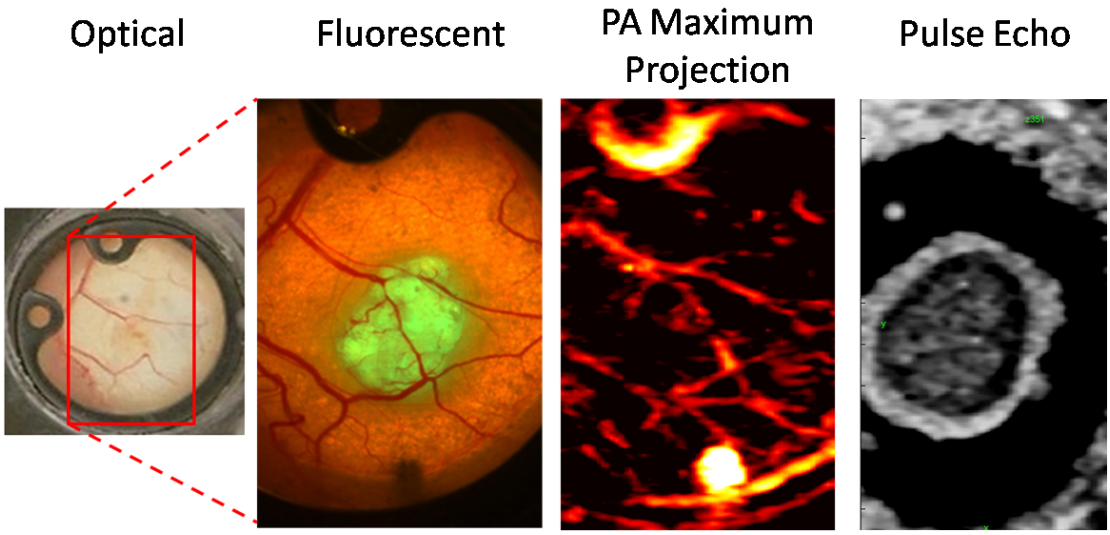

Figure 8. From left to right, optical (Day 9), fluorescent (Day 19), PA (λ = 800 nm) maximum depth projection (Day 16), and a PE lateral-lateral plane (Day 16) for mouse R2. Red scale box has dimensions of approximately 6 mm x 11 mm. Location of GFP is revealed in fluorescent image, blood vessel locations are displayed in PA image , and the tumor's depth profile is demonstrated in PE image with a hyperechoic exterior and hypoechoic interior.

Downloaded from SPIE Digital Library on 04 Apr 2010 to 150.135.114.25. Terms of Use: http://spiedl.org/terms

The PE image on the right of Figure 8 provides complementary contrast information that can be compared with the fluorescent image, including the tumor size (see previous section) and microstructure during a tumor invasion. In this example, the PE image (lateral XY plane near top of tumor rendered from the 3D PE dataset) provides information at different depths corresponding with the fluorescent image, and illustrates how the tumor protrudes outward from the skin surface (away from the coverslip and in the region of the GFP signals). The PE image also portrays an outer ring of the tumor that appears hyperechoic, while the bulk tumor appears hypoechoic. This is consistent with the dynamic processes that occur during tumor growth. In short, 3D PA and PE imaging offer complementary contrast mechanisms related to the microenvironment and blood vessels during a tumor invasion.

3.4 Spectroscopic Photoacoustic Imaging

Spectroscopic photoacoustic imaging provides functional information related to blood oxygen saturation and exploits our wavelength tunable laser to map the differential optical absorption properties of the tumor microenvironment as a function of the laser wavelength. Oxygenated and deoxygenated hemoglobin have very different optical absorption spectral profiles, especially in the visible and NIR[16]. Calculating the PA signal's slope within this range is a strong indicator of blood oxygen saturation based on the well known properties of the oxygen dependence on the optical absorption spectrum of hemoglobin. Here, we provide a first-order linear fit of the magnitude of the PA signal at each pixel as a function of wavelength. The slope of each pixel is displayed as an image in Figure 9 (bottom) on a hot cold color scale, with only the most significant slopes above the black background (35 dB dynamic range).

Photoacoustic spectroscopy is a powerful tool for mapping out the oxygenation levels of blood noninvasively. The slope of the spectroscopic PA signal between 680 and 900 nm is displayed (hot/cold, 30 dB) with regions of interest marked with 'A' and 'B' in Figure 9 (bottom). The middle image of Figure 9 displays the PA and PE images at 800 nm. Two pixel regions (examples) with different optical absorption spectrum properties are denoted by "A" and "B.". The results from Figure 9 (bottom) indicate broad areas of de-oxygenated blood (blue/cyan regions), suggesting the presence of hypoxia, a commonly present condition in the tumor microenvironment.

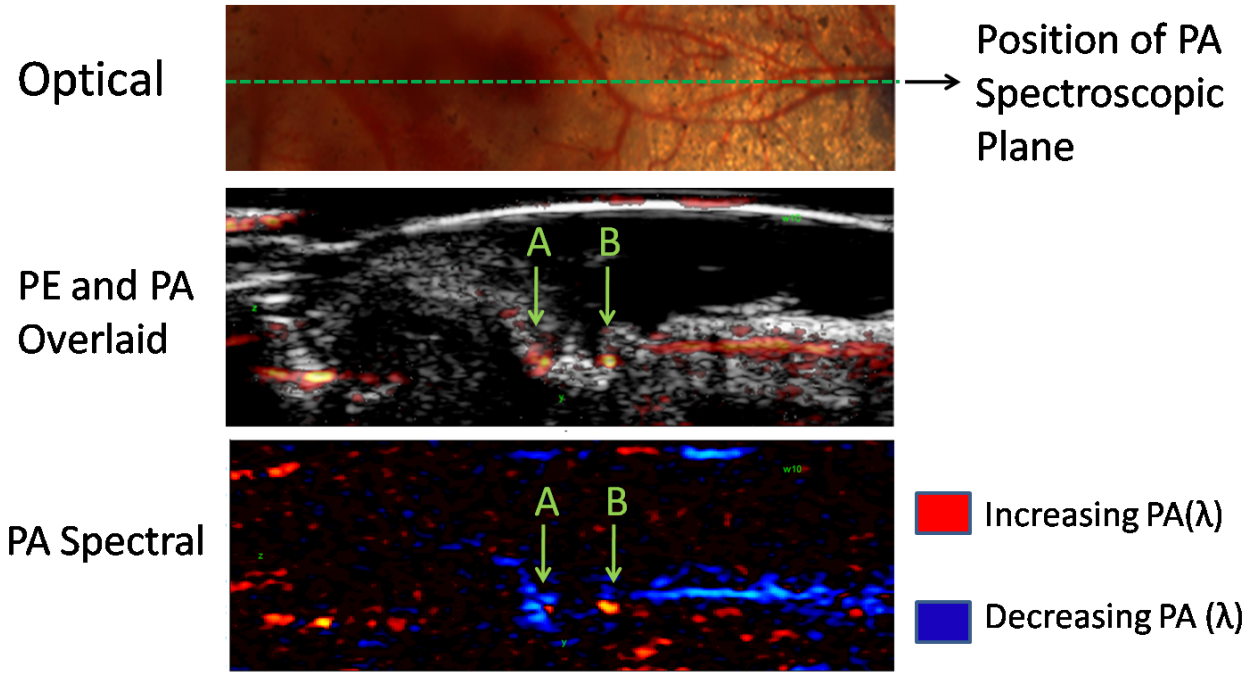

Figure 9. (top) Optical image of the window chamber for mouse R0 on Day 12. (middle) PA image (hot, 20 dB) from Day 29 for 800 nm incident light superimposed on the accompanying PE image (gray, 35 dB). (bottom) Spectroscopic PA slope between 680 and 900 nm demonstrating areas of increasing (red) and decreasing (blue) signal as calculated from a first-order linear fit (hot/cold, 30 db).

Downloaded from SPIE Digital Library on 04 Apr 2010 to 150.135.114.25. Terms of Use: http://spiedl.org/terms

The spectroscopic PA signal obtained from a small ROI surrounding the two points of interest A and B is depicted in Figure 10. The spectral signature of region A matches the absorption spectrum of deoxygenated hemoglobin, while the spectral signature of region B matches that of oxygenated hemoglobin. This powerful technique not only provides detailed noninvasive imaging of the tumor vascular network but also provides functional information concerning the hypoxic condition of the tumor's microenvironment.

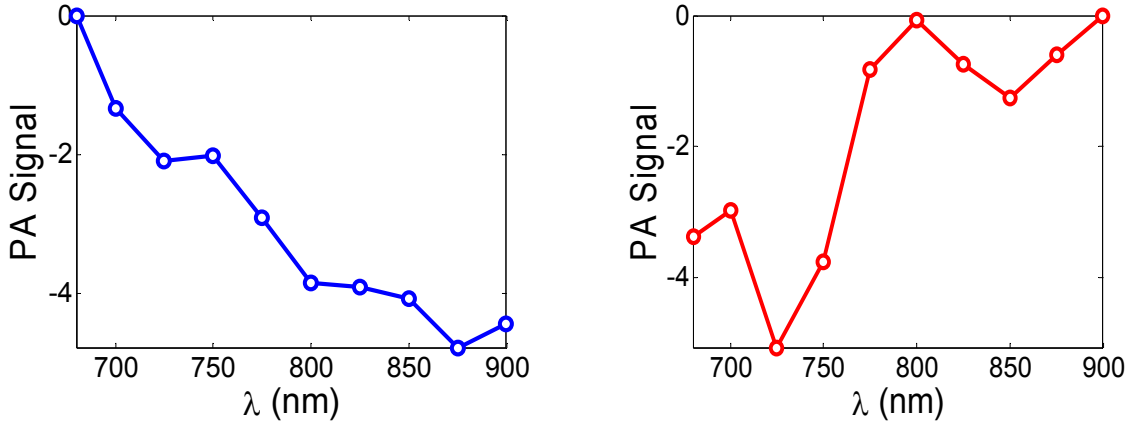

Figure 10. Spectroscopic PA plots for regions of interest A (left) and B (right) depicted in Figure 9 placed on a dB scale (relative to max). Regions A and B match the absorption spectrum of deoxygenated and oxygenated hemoglobin, respectively.

CONCLUSION

We described a novel high resolution, dual-modality pulse echo and photoacoustic imaging system for tracking prostate tumor growth in live mice. Pulse echo ultrasound indicated 3 to 5 fold increase in tumor volume during 3+ weeks of imaging; PE imaging also helped visualize the tumor's microstructure and hypoechoic inner core. Photoacoustic imaging and spectroscopy, on the other hand, provided depth information concerning the tumor's comprehensive vascular network and functional information regarding blood oxygen saturation in the tumor microenvironment, suggesting possible hypoxic regions. Finally, pulse echo and photoacoustic results were compared and validated with optical and fluorescent imaging. Understanding the tumor microenvironment is critical to characterizing how cancers function and determining how they will respond to potential treatment

ACKNOWLEDGMENTS

Support from NSF grant 0853618, Advanced Research Institute for Biomedical Imaging (ARIBI), Technology and Research Initiative Funding (TRIF), Arizona Cancer Center Seed Grant IRG-7400128, Zonare Medical Systems and the National Institutes of Health (NIH). Special thanks to Christy Howison for aiding in animal preparation, as well as to Mir Salek and Art Gmitro's Biomedical Imaging Laboratory for access and assistance to fluorescent imaging.

Downloaded from SPIE Digital Library on 04 Apr 2010 to 150.135.114.25. Terms of Use: http://spiedl.org/terms

REFERENCES

[1] Meehan KL, Holland JW, Dawkins HJS. "Proteomic analysis of normal and malignant prostate tissue to identify novel proteins lost in cancer," Prostate 50(1), 54-63. (2001)

[2] Dennis LK, Resnick Martin I. "Analysis of recent trends in prostate cancer incidence and mortality," The Prostate 42(4),247-52. (2000).

[3] Majeed A, Babb P, Jones J, Quinn M., "Trends in prostate cancer incidence, mortality and survival in England and wales 1971-1998," BJU Int 85(9), 1058-62. (2000)

[4] Threlfall TJ, English DR, Rouse IL. "Prostate cancer in Western Australia: Trends in incidence and mortality from 1985 to 1996," The Medical Journal of Australia 169(1),9-10 (1998)

[5] American cancer society <http://www.cancer.org/docroot/cri/content/cri_2_4_1x_what_are_the_key_statistics_for_prostate_cancer_36.asp.>

[6] Meyer DE, Kong GA, Dewhirst MW, Zalutsky MR, Chilkoti A., "Targeting a genetically engineered elastin-like polypeptide to solid tumors by local hyperthermia," Cancer Research 61(4), 1548-1554. (2001)

[7] Helmlinger G, Yuan F, Dellian M, Jain RK., "Interstitial pH and pO2 gradients in solid tumors in vivo: High-resolution measurements reveal a lack of correlation," Nat Med 3(2), 177-182. (1997)

[8] Oh P, Borgstrom P, Witkiewicz H, Li Y, Borgstrom BJ, Chrastina A, et al., "Live dynamic imaging of caveolae pumping targeted antibody rapidly and specifically across endothelium in the lung," Nat Biotechnol 25(3), 327-337. (2007)

[9] Dewhirst MW, Ong ET, Braun RD, Smith B, Klitzman B, Evans SM, et al., "Quantification of longitudinal tissue pO2 gradients in window chamber tumours: Impact on tumour hypoxia," Br J Cancer 79(11), 1717-22. (1999)

[10] Erickson K, Braun RD, Yu D, Lanzen J, Wilson D, Brizel DM, et al., "Effect of longitudinal oxygen gradients on effectiveness of manipulation of tumor oxygenation," Cancer Research 63(15), 4705-12. (2003)

[11] Yuxiang L, Salek MFS, Jennings N, Gmitro AF., "An optical imaging system for window chambers in MRI system," SPIE 6849, 07 (2008)

[12] Gmitro AF, Lin Y, Salek MF., "A system for multi-modality optical and MR imaging of implanted window chambers," Novel Techniques in Microscopy, (2009)

[13] Dewhirst MW, Ong ET, Klitzman B, Secomb TW, Vinuya RZ, Dodge R, et al., "Perivascular oxygen tensions in a transplantable mammary tumor growing in a dorsal flap window chamber." Radiation Research 130(2), 171-182. (1992)

[14] Wood MFG, Ghosha N, Wallenburga MA, Moriyamaa EH, Lib S, Weiselb RD, et al., "Turbid polarimetry for tissue characterization," SPIE 7371, 06 (2009)

[15] Chomas JE, Pollard RE, Sadlowski AR, Griffey SM, Wisner ER, Ferrara KW. "Contrast-enhanced US of microcirculation of superficially implanted tumors in rats," Radiology 229(2),439-446. (2003)

[16] Faber Dirk J, Mik Egbert G, Aalders Maurice C G, van Leeuwen Ton G, "Light absorption of (oxy-)hemoglobin assessed by spectroscopic optical coherence tomography." Optics Letters 28(16), 1436-1438. (2003)

Downloaded from SPIE Digital Library on 04 Apr 2010 to 150.135.114.25. Terms of Use: http://spiedl.org/terms